Journal of the Mechanical Behavior of Biomedical Materials 167 (2025) 106964

Contents lists available at ScienceDirect

Journal of the Mechanical Behavior of Biomedical Materials

journal homepage: www.elsevier.com/locate/jmbbm

Research paper

# Performance parity in cartilage repair: SPMK-g-PEEK versus cartilage–cartilage interfaces

Robert J. Elkington [a,*], Gregory M. Pryce [a], David Keeling [b], Richard M. Hall [c], Andrew R. Beadling [c], Hemant Pandit [d], Michael G. Bryant [c,1]

[a] Institute of Functional Surfaces, Mechanical Engineering, University of Leeds, Leeds, LS2 9JT, Yorkshire, UK
[b] Key Engineering Solutions Limited, Leeds, LS2 3AA, Yorkshire, UK
[c] School of Engineering, College of Engineering and Physical Sciences, University of Birmingham, Birmingham, B15 2TT, West Midlands, UK
[d] Leeds Institute of Rheumatic and Musculoskeletal Medicine, Chapel Allerton Hospital, Chapeltown Road, Leeds, LS7 4SA, Yorkshire, UK

ARTICLE INFO

*Keywords:*
Polymer brushes
Cartilage
Tribological rehydration
Biphasic lubrication
Aqueous lubrication
BioTribology

ABSTRACT

Effective fluid exudation and rehydration are essential for the low-friction function of healthy articular cartilage, facilitating interstitial fluid pressurisation, solute transport, and aqueous lubrication. However, current metallic biomaterials used in focal cartilage repair or hemiarthroplasty compromise this fluid-pressure dependent load support, leading to the erosion of the interfacing cartilage. This study investigates bioinspired hydrophilic 3-sulfopropyl methacrylate potassium salt (SPMK) polymer grafted onto a PEEK substrate (SPMK-g-PEEK) as a potential solution. SPMK-g-PEEK aims to mimic the natural tribology of cartilage by providing an aqueous low friction interface and polyelectrolyte-enhanced tribological rehydration (PETR), supporting fluid recovery and interstitial fluid pressurisation during cartilage sliding. We compare the tribological characteristics of physiological cartilage–cartilage interfaces, which rely on osmotic swelling and hydrodynamic tribological rehydration, with PETR enabled by SPMK-g-PEEK interfaces.

This study introduces a bespoke Fuzzy-PI controlled biotribometer. Employing a dual-phase testing method, static compression followed by sliding, allows simultaneous measurement of friction and cartilage strain recovery, indicative of interstitial fluid recovery following compressive exudation. Cartilage condyle, unfunctionalised PEEK, and SPMK-g-PEEK surfaces were investigated against flat cartilage plugs, which provide no hydrodynamic entrainment zone for tribological rehydration, and convex cartilage plugs, which create a convergent hydrodynamic zone for tribological rehydration. Matched cartilage–cartilage contacts exhibited low friction coefficients of ~ 0.04 and strain recovery of up to ~ 14% during the sliding phase. SPMK-g-PEEK surfaces sliding against convex cartilage plugs demonstrated similar strain recovery of ~ 13% and reduced friction coefficients of ~ 0.01, due to the combined effects of PETR and hydrodynamic tribological rehydration. In contrast, unfunctionalised PEEK surfaces, similar to current hard biomaterials employed in cartilage resurfacing, showed significantly higher friction and inhibited rehydration. SPMK-g-PEEK effectively mimics the physiological rehydration of connatural articular cartilage surfaces, highlighting its potential as a biomimetic material for cartilage resurfacing.

## 1. Introduction

Articular cartilage is the specialised, avascular connective tissue that lines the surfaces of synovial joints, providing low friction, and load-bearing properties crucial for joint mobility throughout the human lifespan (Lin and Klein, 2021). Structurally, cartilage is a biphasic poro-viscoelastic material, composed of an approximately 80% interstitial fluid phase and 20% solid matrix primarily composed of collagen and hydrophilic proteoglycans, with embedded chondrocytes that maintain the extracellular matrix (Sophia Fox et al., 2009). Additionally, the cartilage surface is coated with a supramolecular complex of biopolyelectrolytes, including lubricin and hyaluronic acid, which provide boundary lubrication (Lin and Klein, 2021; Cederlund and Aspden, 2022; Elkington et al., 2024a). Under loading and articulation, the interstitial fluid within the collagen extracellular matrix pressurises (Cederlund and Aspden, 2022), supporting up to 90% of the joint load and partially exuding to form a lubricating fluid film (Krishnan et al., 2004;

* Corresponding author.
*E-mail addresses:* mnrje@leeds.ac.uk (R.J. Elkington), m.g.bryant@bham.ac.uk (M.G. Bryant).
[1] Senior author.

https://doi.org/10.1016/j.jmbbm.2025.106964
Received 19 October 2024; Received in revised form 25 February 2025; Accepted 1 March 2025
Available online 13 March 2025
1751-6161/© 2025 The Authors. Published by Elsevier Ltd. This is an open access article under the CC BY license (http://creativecommons.org/licenses/by/4.0/).

Soltz and Ateshian, 1998). Synovial joints are subjected to spatially averaged and peak loads ranging from 0.75 to 20 MPa, resulting in the sustained exudation of interstitial fluid from cartilage under load. Consequently, intrinsic mechanisms for fluid recovery are essential to maintain joint function (Eckstein et al., 1999; Moore and Burris, 2017). *In vivo* studies demonstrate that cartilage experiences low strains ($\varepsilon$ = 3%–10% Eckstein et al., 1999; Cutcliffe et al., 2020) during physical activity, whereas periods of inactivity leads to high strains in excess of $\varepsilon \sim 50\%$ (Herberhold et al., 1999). Cartilage rehydration is expected to occur through osmotic swelling during transient periods of loading, fluid confinement in the contact gap, and sliding induced *tribological rehydration* where fluid is pressurised between conformal articular surfaces leading to hydrodynamic pressurisation induced fluid recovery (Moore and Burris, 2017; Moore, 2017; Caligaris and Ateshian, 2008; Voinier et al., 2022).

The competing roles of fluid rehydration and exudation are essential for the tribological (low friction and wear prevention Ateshian, 2009; Forster and Fisher, 1999; Moore and Burris, 2015), mechanical (load support and matrix stress shielding Ateshian, 2009; Moore et al., 2017; Accardi et al., 2011) and biological (solute transport, cellular mechanotransduction Graham et al., 2017; Schätti et al., 2016; Albro et al., 2008; Zhao et al., 2020) functions of articular cartilage. Inhibited interstitial fluid recovery disrupts homeostasis, leading to increased cartilage strain, wear, and friction and eventually excessive joint space narrowing (Moore and Burris, 2017; Rajankunte Mahadeshwara et al., 2024), a common indicator of joint disease and pathogenesis of osteoarthritis due to compounding cartilage erosion (Fife et al., 1991; Cooper et al., 2000). This, due to the limited ability of avascular cartilage to heal, can eventually require clinical interventions such as total joint replacement (TJR) (Van Herck et al., 2010). The escalating global incidence of symptomatic osteoarthritis is creating a substantial health burden (Maiese, 2016; Rajankunte Mahadeshwara et al., 2024), characterised by a rising number of patients under 65 undergoing joint replacement, with many later requiring costly revision surgeries (Kurtz et al., 2009; Weber et al., 2018). To reduce TJR and revision surgeries, early, less invasive interventions such as focal cartilage repair devices or tissue engineering approaches are being developed to restore articular cartilage tissue and function (Brittberg et al., 2016; Mastbergen et al., 2013). However, tissue engineering approaches have limited clinical adoption due to restrictive clinical indications (Makris et al., 2015; Liu et al., 2017). Whereas, the current reliance on hard metallic or ceramic biomaterials for focal cartilage repair compromises fluid load support leading to wear of the opposing cartilage surface (Dabiri and Li, 2015; Pawaskar et al., 2011; Diermeier et al., 2020), offering only short-term benefits (Jeuken et al., 2021; Jermin et al., 2015). Requiring a class of materials to be developed informed by the native tribology of articular cartilage which provide effective fluid load support and interstitial fluid recovery (Tan et al., 2023).

The tribological function of cartilage has been experimentally and theoretically described by interstitial fluid pressurisation (IFP) theory (Krishnan et al., 2004; Soltz and Ateshian, 1998). More complex computational models treat cartilage as a porohyperelastic material or utilise finite element analysis to capture the multiscale lubrication behaviour across different lubrication regimes (De Boer et al., 2020; Putignano et al., 2021). While such approaches offer further insights, our focus here is on IFP theory to examine interstitial fluid exudation and reuptake, aligning with the experimental framework described later in this paper (Moore, 2017; Burris and Moore, 2017). The coefficient of friction (CoF, $\mu$) of cartilage is determined by the relationship between cartilage strain ($\varepsilon(t)$) or fluid load fraction ($F'$), and their equilibrium parameters corresponding to zero interstitial pressure ($\mu_{eq}$, $\varepsilon_{eq}$), as described by Eq. (1) (Krishnan et al., 2004; Soltz and Ateshian, 1998; Moore et al., 2017). Simply, low cartilage friction necessitates sustained hydration to modulate low strain ($\varepsilon$) and high fluid support ($F'$).

$$\mu(t) = \mu_{eq}\frac{\varepsilon(t)}{\varepsilon_{eq}} = \mu_{eq}(1 - F') \tag{1}$$

*In vitro* tribological studies have accurately modelled osmotic swelling behaviour utilising a *migrating contact area* (MCA) approach, where a glass probe slides across a cartilage plate, indefinitely maintaining physiological CoF within the range of 0.01 - 0.03 (McCutchen, 1962; Caligaris and Ateshian, 2008). Moore and Burris have demonstrated similar maintenance of physiological CoF levels below 0.03 by utilising a *convergent stationary contact area* (cSCA) convex cartilage explant sliding over a glass plate. Elucidating tribological rehydration, a second mechanism of cartilage fluid recovery, onset by sliding and independent of contact migration or unloading (Moore and Burris, 2017; Burris and Moore, 2017; Kupratis et al., 2021). This requires sliding speeds exceeding $\sim$ 30 mm/s to generate hydrodynamic pressures at the cSCA's wedge-shaped leading edge, promoting fluid influx into the cartilage (Moore and Burris, 2017; Putignano et al., 2021). Experimental observations of cSCA tribological rehydration are illustrated in Fig. 1, demonstrating that following a period of compressive strain ($\varepsilon_C$), sliding triggers strain recovery attributable to cartilage rehydration ($\varepsilon_{cSCA} < \varepsilon_C$) and hence sustained fluid load support ($F'$) and low friction ($\mu < 0.03$) (Elkington et al., 2024b; Farnham et al., 2021; Kupratis et al., 2021). In contrast, a flat *stationary contact area* (SCA) cartilage explant exhibits no rehydration and strain continues to increase throughout sliding ($\varepsilon_{SCA} > \varepsilon_C$ as $\varepsilon_{SCA} \rightarrow \varepsilon_{eq}$), leading to increasing CoF ($\mu \rightarrow \mu_{eq}$) (Elkington et al., 2024b, 2023; Kupratis et al., 2021). This configuration is analogous to unconfined compression with no capacity for fluid recovery to compete with compressive exudation, resulting in diminishing fluid load support ($F'$) (Moore et al., 2017; Caligaris and Ateshian, 2008; Elkington et al., 2024b).

Presently there are ongoing efforts to develop materials systems that can mimic the hydrophilic composition of the cartilage extracellular matrix and facilitate fluid recovery and load support, exploiting high water content materials such as hydrogels or polymer brushes (Tan et al., 2023; Kyomoto et al., 2010; Yang et al., 2020). Recent studies by Elkington et al. (2023, 2024b,a) have investigated 3-sulfopropyl methacrylate potassium salt (SPMK) grafted to a PEEK substrate (SPMK-g-PEEK) as a bioinspired material for focal cartilage repair. This material features a 350 nm thick coating of SPMK polymer end-tethered to the PEEK substrate. The high concentration of hydrophilic anionic sulfonic acid groups swell up to a ~5 μm thickness in aqueous environments, mimicking the biopolyelectrolytes native to articular cartilage (Elkington et al., 2023, 2024a). The hydrated surface of SPMK-g-PEEK provides effective aqueous boundary lubrication along with a fluid reservoir to support rehydration of cartilage surfaces (Elkington et al., 2024a, 2023). Which can sustain CoF < 0.01 and strain recovery indicative of fluid rehydration sliding against SCA cartilage from sliding speeds as low as 0.5 mm/s (Elkington et al., 2023, 2024b,a). Introducing an engineered mechanism of cartilage interstitial fluid recovery, *polyelectrolyte-enhanced tribological rehydration* (PETR), attributed to polyelectrolyte enhanced elastohydrodynamic lubrication and fluid pressurisation during compression of sulfonic acid hydration shells (Elkington et al., 2024a,b).

For synovial joints cartilage fluid recovery has widely been attributed to articulation induced free swelling at exposed surfaces (Voinier et al., 2022; Linn, 1967). Passive swelling, free swelling of unloaded articular cartilage, refers to the osmotic-driven expansion of cartilage in the absence of contact with the opposing joint surface (i.e. a migrating contact area). However, across the macro-scale cartilage contact area, *in vivo* studies demonstrate cartilage often remains in contact during unloading of periodic activities (e.g. gait) (Hinterwimmer et al., 2005; Henderson et al., 2011), limiting the extent of passive swelling and indicating that additional mechanisms contribute to fluid recovery and sustained pressurisation. Comparative studies highlight that tribological rehydration can replenish cartilage fluid at a rate up to 7× greater than passive swelling alone (Voinier et al., 2022). Computational models suggest that fluid exchange and synovial rehydration in the cartilage contact gap occurs due to interfacial gaps formed by opposing rough cartilage surfaces ($R_a \sim 2.0$ μm) (Wu and

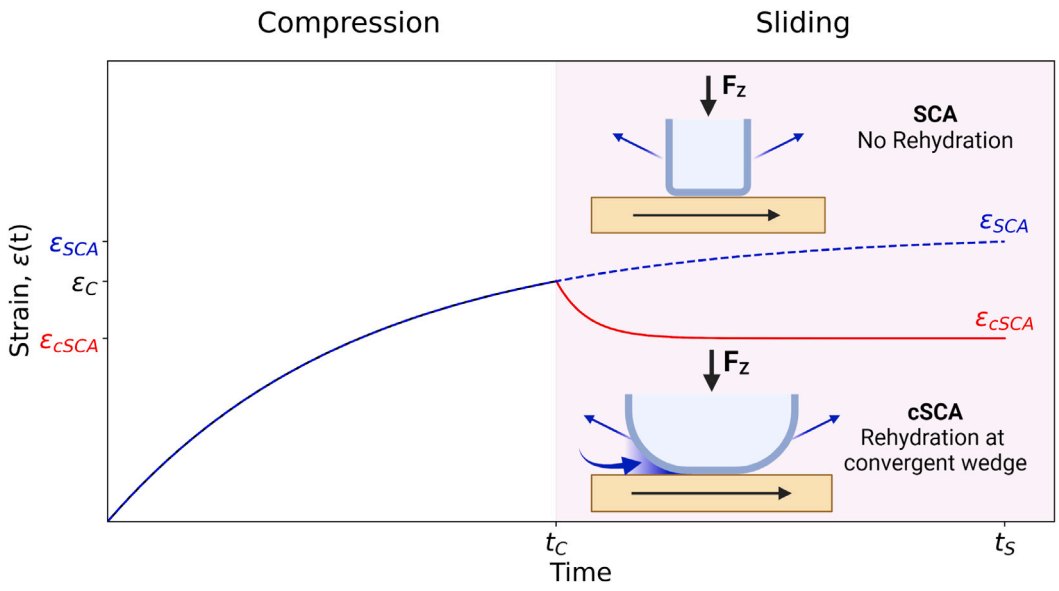


**Fig. 1.** Illustrative strain profile for a cSCA and SCA cartilage explants undergoing a period of compression-strain ($\varepsilon_C$), followed by sliding-under-compression against a hard impermeable substrate. Upon sliding, the cSCA cartilage explant recovers strain ($\varepsilon_{cSCA} < \varepsilon_C$ as $\varepsilon_{SCA} \rightarrow \varepsilon_{eq}$) through tribological rehydration, facilitated by hydrodynamic fluid pressurisation at the convergent wedge leading edge. In contrast, the SCA cartilage explant is analogous to unconfined compression, with no capacity for rehydration, and strain increases throughout sliding diminishing interstitial fluid pressurisation. Blue arrows indicate interstitial fluid flow.

Ferguson, 2017; Liao et al., 2019; Putignano et al., 2021). However, the interplay between synovial rehydration (i.e. fluid exchange and osmotic swelling) within the cartilage contact gap and the macroscale geometry enabling tribological rehydration in conformal synovial joints has yet to be investigated directly.

Free swelling (MCA) cartilage rehydration has been demonstrated with matched cartilage–cartilage interfaces demonstrating sustained low CoF, but does not elucidate additional rehydration behaviours (i.e. measure strain) (Caligaris and Ateshian, 2008). Tribological rehydration has only been shown in a cSCA configuration against impermeable (glass) interfaces to isolate the effects of free swelling, demonstrating both sustained low CoF and strain recovery (Moore et al., 2017; Farnham et al., 2021). PETR has been demonstrated with SCA cartilage interfaced with SPMK-g-PEEK, isolating the hydrodynamic effects of conventional tribological rehydration (Moore, 2017), demonstrating both strain recovery and low CoF due to effective aqueous boundary lubrication (Elkington et al., 2023, 2024b,a). The SPMK polyelectrolyte interface enhances fluid confinement and pressurisation in the contact gap to augment fluid exchange within the loaded contact area (Elkington et al., 2024a,b).

This study aims to establish an *in vitro* expanded testing framework presented in Fig. 1, comparing strain recovery indicative of rehydration in matched cartilage–cartilage contacts with that of cartilage paired with materials designed to enhance rehydration (SPMK-g-PEEK). There are limited studies of cartilage–cartilage interfaces, partly due to the uncertainty and challenges introduced by uneven and compliant condyle surfaces, and are limited to only studying friction rather than strain (Forster and Fisher, 1996; Schmidt et al., 2007; Trevino et al., 2017; Caligaris and Ateshian, 2008). The initial phase of the study will concentrate on quantifying tribological and fluid recovery properties of cartilage–cartilage interfaces, requiring precise adaptive load control to accommodate the dynamic nature of cartilage strain and contact area during sliding (Schätti et al., 2016). Subsequently, this will then be used as a comparative benchmark to SPMK-g-PEEK and unfunctionalised PEEK control surfaces mated against SCA and cSCA cartilage. This aims to compare hydrodynamic tribological rehydration of hard impermeable biomaterials against the combined action of PETR and hydrodynamic tribological rehydration facilitated with SPMK-g-PEEK. This approach seeks to quantitatively evaluate if SPMK-g-PEEK is a viable focal cartilage repair surface for reproducing physiological cartilage–cartilage interstitial fluid recovery and low friction.

## 2. Methods

### 2.1. Materials

Polyether-ether-ketone (PEEK) 450G, procured from Victrex (UK) was initially received in the form of flat sheets with a thickness of 5 mm. These were subsequently sectioned into square samples measuring 25 × 25 mm, and underwent polishing to achieve a surface roughness ($R_a$) of 30 nm. The monomer 3-sulfopropyl methacrylate potassium salt (SPMK), with a purity greater than 98%, along with phosphate-buffered saline (PBS) tablets, were obtained from Sigma Aldrich, United Kingdom, and used without further modification. PEEK substrates were surface functionalised by UV photopolymerisation grafting-from of SPMK monomer to produce SPMK-g-PEEK. These methods were established and are fully detailed in a previous publication (Elkington et al., 2023). PBS was used as a storage and lubrication medium throughout cartilage tribological testing to mimic the osmolarity found in physiological conditions.

Bovine stifle specimens sacrificed at approximately 2 years of age were procured from John Penny & Sons abattoir, Leeds, UK and received on the same day of butchery. Cartilage was exclusively harvested from the femoral side of the stifle joints. Approximately planar cartilage plates (~20 × 30 mm) were cut from the patellofemoral grooves of stifle joints using a high speed 18,000 rpm oscillating saw. Flat SCA cartilage samples were also extracted from the patellofemoral groove using a 35,000 rpm 7.2 mm internal diameter trephine bur and cooled with PBS during extraction. Larger cSCA explants were harvested from the lateral and medial femoral condyles using a 20 mm holesaw with an internal diameter of 18 mm. These methods and explant dimensions follow previous work which obtain flat ⌀7.2 mm SCA contacts (Elkington et al., 2024a,b) and convex ⌀18 mm cSCA contacts (Burris and Moore, 2017; Moore, 2017). Any samples with surface defects or SCA samples with a planar height difference of > 0.1 mm were discarded. Following extraction all cartilage samples were cryopreserved (−18 °C) in PBS for up to one week, prior to testing samples were thawed for at least 12 h in a refrigerator followed by acclimatisation to room temperature for an additional 2 h. Cryopreservation of cartilage samples up to (−20 °C) for up to one week has been shown not to significantly affect surface properties, including roughness, collagen fibril alignment, or the coefficient of friction (Espinosa et al., 2021).

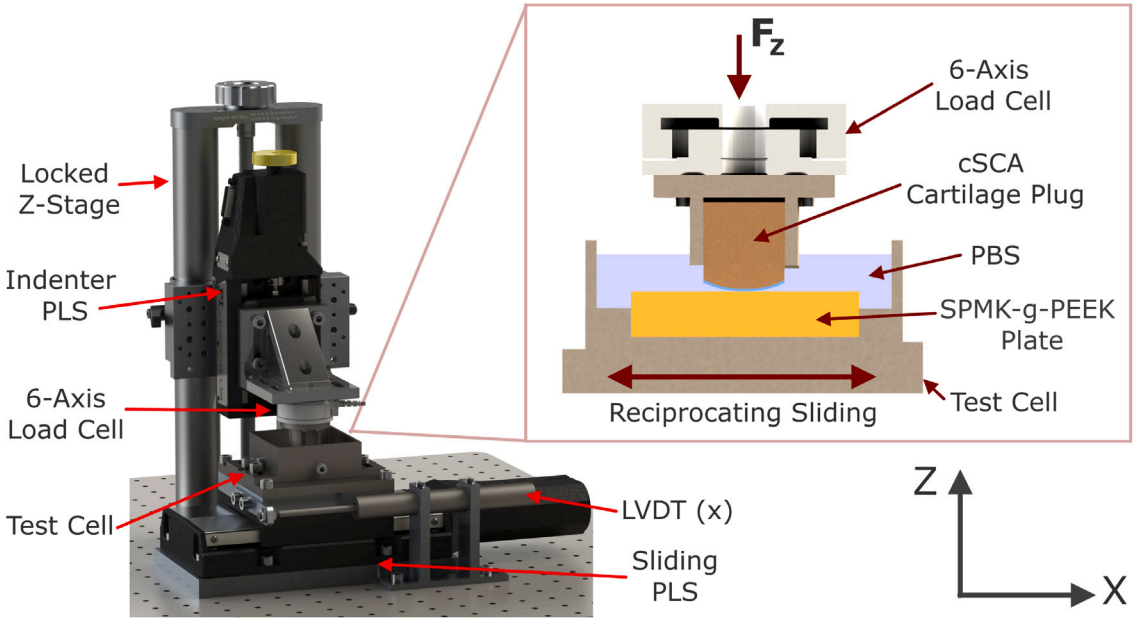


**Fig. 2.** Schematic of the Fuzzy-PI tribometer instrumented with load cell, indenter and sliding PLS, and LVDT labelled with callout view of test cell show cSCA cartilage sliding against a SPMK-g-PEEK plate submerged in PBS.

### 2.2. Fuzzy-PI enabled tribometer

Fig. 2 shows the bespoke tribometer employing two Precision Linear Stages (PLS) (Phyisk Instrumente GmbH and Co, Germany); an indenter PLS ($Z$-axis, L-509 Precision Linear Stage) to apply normal force and a sliding PLS ($X$-axis, L-511 High-Precision Linear Stage) to facilitate sliding perpendicular to the direction of loading. The indenter PLS has a maximum velocity of 20 mm/s, the larger sliding PLS has a maximum velocity of 90 mm/s with linear position ($X$) tracked by a Linear Variable Differential Transformer (LVDT) with a resolution of 0.1 μm. A six-axis load cell (ATI Industrial Automation Inc, USA) was mounted perpendicular to the test cell along with a cartilage plug mount, fixed to the stage of the indenter PLS. The load cell can measure maximum loads of 145 N with a resolution of 0.05%, in this setup only the forces in the $Z$ and $X$ directions were used to measure the normal force ($F_Z$) and tangential force ($F_X$) respectively. A detailed schematic of the test cell is also shown in Fig. 2 showing a cSCA cartilage plug mounted on the 6-axis load cell with a SPMK-g-PEEK plate submerged in PBS in the test cell bath. This setup was controlled using a custom LabVIEW programme interfaced with a CompactRIO embedded controller (National Instruments, USA). Normal force ($F_Z$) was maintained throughout testing using Fuzzy-PI control (Iyer et al., 2024). The advanced controller integrates a Fuzzy 'supervisor' with a PI 'slave' in a synergistic manner. As the system operates, the error generated by the PI controller is used as an input variable for the Fuzzy controller. The interface engine of the Fuzzy controller then calculates the new Proportional (P) and Integral (I) gains in real time, which the PI controller uses to dynamically adjust its feedback parameters. The PI controller ran on the FPGA of the compactRIO at 10 kHz, whilst the Fuzzy-Logic supervisor ran in real-time on the same device at 100 Hz. This approach ensures that the controller adapts to the changing cartilage contact deformation resulting from temporal variations in hydration and strain during testing.

### 2.3. Experimental overview

To evaluate the tribological performance and rehydration characteristics, both the SCA (no tribological rehydration) and cSCA (tribological rehydration) cartilage pins were subjected to a rehydration cycle comprising of a compression phase followed by sliding. These tests were conducted against three distinct substrates: a physiological control of a condyle plate (synovial rehydration), unfunctionalised PEEK (no PETR rehydration), and SPMK-g-PEEK (PETR rehydration). The rationale for each substrate–cartilage pin combination are summarised in Table 1.

**Table 1**
Overview of rehydration cycle experiments conducted with SCA and cSCA cartilage pins against cartilage condyle, unfunctionalised PEEK, and surface modified SPMK-g-PEEK substrates.

| Pin geometry–substrate contact | Rehydration mechanisms |
|---|---|
| SCA-Condyle (N = 3) | Synovial rehydration |
| cSCA-Condyle (N = 3) | Tribological + Synovial rehydration |
| SCA-PEEK (N = 3) | No rehydration |
| cSCA-PEEK (N = 3) | Tribological rehydration |
| SCA-SPMK (N = 3) | PETR |
| cSCA-SPMK (N = 3) | Tribological + PETR rehydration |

Akin to Fig. 1, the rehydration cycle consisted of an 1800 s compression period ($0 \leq t < 1800$ s) followed by 1800 s of reciprocating sliding ($1800 \leq t \leq 3600$ s) at a frequency of 1 Hz over a 10 mm linear sliding distance. Throughout the whole rehydration cycle a constant normal load of 20 N was maintained using Fuzzy-PI control (Iyer et al., 2024). The contact pressure under a 20 N load across a 7.2 mm diameter flat SCA is calculated to be approximately 0.50 MPa. This estimate is also consistent for the larger 18 mm convex cSCA, where optical measurements against impermeable surfaces (glass) suggest a similar effective contact area of about ~7 mm (Burris and Moore, 2017), resulting in a comparable contact pressure of 0.50 MPa. These values fall within the typical physiological spatially and temporally averaged contact stresses in the range of 0.1–2.0 MPa for mammalian joints (Brand, 2005; Elkington et al., 2023). All tests were conducted in a fully submerged phosphate-buffered saline (PBS) environment, selected for its dual functions. PBS maintained osmotic conditions that prevented undue cartilage swelling or shrinkage, closely mimicking the osmolarity experienced *in vivo*. Additionally, it served as an aqueous medium to facilitate cartilage rehydration during the sliding phase. Pin–substrate testing order was randomised to minimise potential systemic biases.

#### 2.3.1. Sliding and measurement of coefficient of friction

The tribometer enabled reciprocating sliding motion at 1 Hz, with a linear displacement ($X$) of ± 10 mm and a peak velocity of 31.4 mm/s.

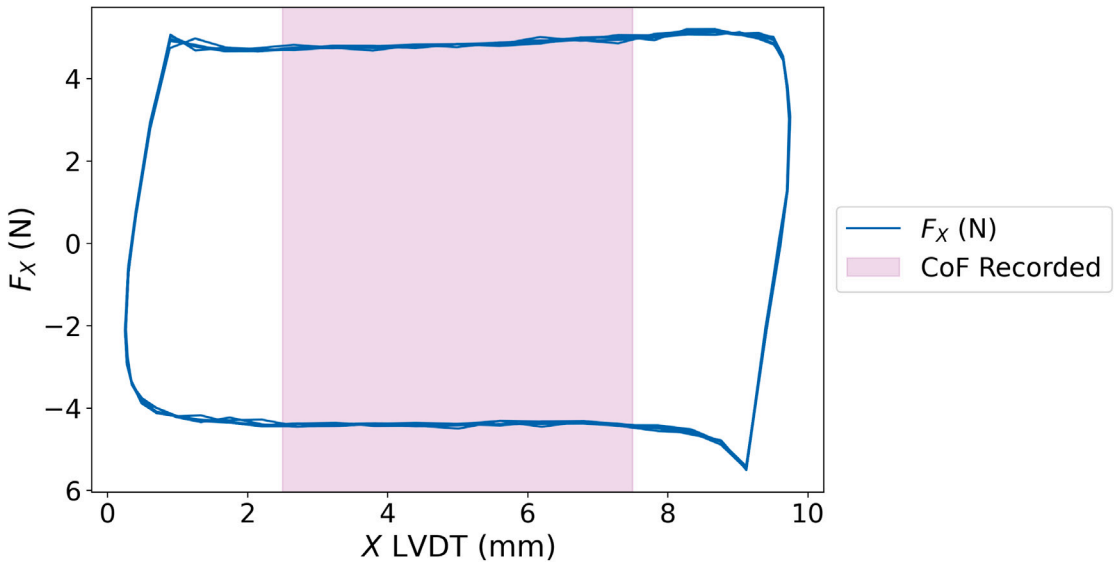


**Fig. 3.** Representative plot of $X$ displacement versus tangential force ($F_X$) illustrating the region (shaded) used for calculating the coefficient of friction (CoF) values. CoF is computed as the mean value within this shaded area ($2.5 \leq X \leq 7.5$ mm). This plot depicts five $X$-$F_X$ curves for the cSCA-PEEK condition (Table 1).

To capture the dynamic changes in the Coefficient of Friction (CoF, $\mu$), both normal ($F_Z$) and tangential ($F_X$) forces were sampled at a frequency of 50 Hz. Forces in the perpendicular ($F_Y$) direction were not analysed, as they were typically negligible or below the resolution of the load cell. CoF, Eq. (2), is calculated as the mean value of data sampled during the middle 50% of each linear reciprocation ($2.5 \leq X \leq 7.5$ mm). This range, encompassing the speed range of 22.1 to 31.4 mm/s, is highlighted in the shaded regions of Fig. 3 showing a representative $X$ displacement versus tangential force $F_x$ plot. This specific range can be considered the steady-state period of the sliding cycle. Of particular note are the CoF upon the startup of the sliding cycle ($\mu_S$,$t$ = 1800 s) and the final CoF achieved at the end of sliding ($\mu_F$,$t$ = 3600 s).

$$\mu = \frac{F_x}{F_z} \tag{2}$$

### 2.3.2. Cartilage compression

Vertical displacement was monitored using the PLS inbuilt linear encoder for direct position measuring with a sampling frequency of 5 Hz. Vertical displacement is calculated as the average change in sample height over every five consecutive reciprocating cycles, indicating the strain response of the cartilage pin. Cartilage strain recovery during the sliding phase ($\varepsilon_r(t)$, Eq. (3)) was determined by subtracting the vertical displacement of the contact pair at the start of sliding ($Z(t = 1800$ s)) from the time dependent vertical displacement ($Z(t)$), and normalising this difference by the swollen, uncompressed cartilage height ($h_{\text{cartilage}}$). This quantifies the cartilage strain recovery, attributing positive values of $\varepsilon_r(t)$ to sliding induced interstitial fluid recovery, and negative values to sustained fluid loss exhibited as continued compression. Referring to IFP theory (Eq. (1)), the initial 30-min compression phase aims to induce cartilage strain towards the equilibrium state ($\varepsilon_C \Rightarrow \varepsilon_{eq}$). Therefore, increasing strain recovery ($\varepsilon_r(t)$) during sliding is expected to result in a lower steady-state coefficient of friction ($\mu_F$) compared to the startup coefficient ($\mu_S$).

It is important to note that while SPMK-g-PEEK and PEEK samples are treated as incompressible materials, the compression phase against cartilage condyles results in deformation of both the pin and the condyle surface. Therefore, to measure the change in height attributable to the cartilage pin, the $X$-positions of the deformed condyle following compression phase were excluded from the calculation of average $Z(t)$ displacement. This complicates direct comparison to IFP theory discussed in Eq. (1), as the equilibrium strain ($\varepsilon_{eq}$) of the cartilage plug cannot be precisely determined at the end of the compression phase ($\varepsilon_C$). However, calculation of the overall strain recovery ($\varepsilon_r(t = 3600$ s)), denoted as $\varepsilon_r$, remains consistent with previous protocols utilised to quantify strain recovery attributable to tribological rehydration on cSCA cartilage (Kupratis et al., 2021; Farnham et al., 2021) and PETR of SCA cartilage (Elkington et al., 2024b,a).

$$\varepsilon_r(t) = \frac{Z(t = 1800\text{ s}) - Z(t)}{h_{\text{cartilage}}} \tag{3}$$

### 2.3.3. Statistical analysis

Independent $t$-tests were conducted to compare the mean overall strain recovery ($\varepsilon_r$), startup CoF ($\mu_S$) and final CoF ($\mu_F$) across different contact geometries (Table 3) and substrates (Table 4). The $t$-tests were used to determine if there were significant differences between the means of two independent groups under different conditions. The *t-statistic* quantifies the difference between the sample means in terms of standard deviations; a higher absolute $t$-statistic value indicates a greater difference between the groups. The *p-value* represents the likelihood that the observed differences are due to experimental error. In this study, a significance level of 0.050 was used, meaning $p$-values below 0.050 were considered statistically significant. Normal distribution of the results data was assumed for the conducted statistical analyses. Independent $t$-tests were performed to compare:

- **Contact Geometry**: SCA vs. cSCA for each substrate (PEEK, Condyle, SPMK-g-PEEK), elucidating the contribution of tribological rehydration facilitated by the cSCA contact.
- **Substrate Effects:** PEEK and SPMK-g-PEEK vs. matched cartilage for both SCA and cSCA conditions, elucidating the contribution of substrate hydration to replicate the tribology of matched cartilage (physiological condition).

This statistical approach allows for the quantitative assessment of the effects of geometric and surface interactions on cartilage tribology and rehydration. The full pairwise $t$-tests results across all contact conditions are provided in the supporting information (Tab. A1). Primarily, this approach seeks to determine if PETR (i.e. SPMK-g-PEEK substrates) can mimic native synovial rehydration of matched cartilage (condyle substrates).

**Table 2**
Summary of the mean applied normal load ($F_Z$), mean overall strain recovery ($\varepsilon_r$), mean initial startup CoF ($\mu_S$), and mean final CoF ($\mu_F$) for each test configuration. The values are based on tests conducted in accordance with the parameters specified in Table 1. Each test was performed in triplicate (N = 3), and the data are presented as mean ± one standard deviation.

| Test (N = 3) | Applied load $F_Z$ (N) | Strain recovery $\varepsilon_r$ (%) | Startup CoF $\mu_S$ (–) | Final CoF $\mu_F$ (–) |
|---|---|---|---|---|
| SCA-Condyle | 19.87 ± 1.53 | 8.77 ± 3.10 | 0.133 ± 0.032 | 0.049 ± 0.012 |
| cSCA-Condyle | 19.69 ± 1.39 | 14.11 ± 4.15 | 0.125 ± 0.025 | 0.038 ± 0.020 |
| SCA-PEEK | 19.89 ± 0.81 | −4.69 ± 1.60 | 0.300 ± 0.045 | 0.269 ± 0.064 |
| cSCA-PEEK | 19.77 ± 1.01 | 4.15 ± 1.01 | 0.282 ± 0.069 | 0.148 ± 0.037 |
| SCA-SPMK | 20.21 ± 0.29 | 7.04 ± 1.71 | 0.038 ± 0.024 | 0.011 ± 0.006 |
| cSCA-SPMK | 19.98 ± 0.39 | 12.95 ± 2.55 | 0.043 ± 0.012 | 0.007 ± 0.004 |

**Table 3**
Contact Geometry: Comparison of mean overall strain recovery ($\varepsilon_r$), startup CoF ($\mu_S$) and final CoF ($\mu_F$) between each substrate in SCA and cSCA configurations using independent *t*-tests. The *t*-statistic measures the difference between the sample means in terms of standard deviations, and the *p*-value indicates the statistical significance of the observed differences.

| Sample pair | Strain recovery ($\varepsilon_r$) | | Startup CoF ($\mu_S$) | | Final CoF ($\mu_F$) | |
|---|---|---|---|---|---|---|
| | *t*-statistic | *p*-value | *t*-statistic | *p*-value | *t*-statistic | *p*-value |
| SCA-Condyle vs. cSCA-Condyle | −1.786 | 0.154 | 0.341 | 0.751 | 0.817 | 0.469 |
| SCA-PEEK vs. cSCA-PEEK | −8.092 | 0.003 | 0.378 | 0.727 | 2.835 | 0.061 |
| SCA-SPMK vs. cSCA-SPMK | −3.681 | 0.041 | −0.323 | 0.768 | 0.961 | 0.398 |

## 3. Results & Discussion

Table 2 summarises the mean applied load, $F_Z$ ± one standard deviation, throughout the sliding phase. Variability of applied load was most pronounced when interacting with cartilage condyle surfaces (Supplementary Figure A1) and in the case of the highest strain PEEK conditions leading a maximum deviation of ±1.53 N. The Fuzzy-PI controllers capability to dynamically tune the PI controller (Iyer et al., 2024) was effective in responding to the temporal cartilage deformation and maintaining an approximately constant 20 N load throughout sliding. Notably, matched cartilage tribology studies often do not disclose the normal load error nor state the deviation (Caligaris and Ateshian, 2008; Merkher et al., 2006; Bell et al., 2006; Katta et al., 2007; Northwood et al., 2007). This lack of reporting makes direct comparisons challenging. However, the observed maximum deviation of ± 1.53 N is relatively small (~7.5% of the target load of 20 N), whereas previous studies on matched cartilage have shown that for contact pressures with a 25% difference (ranging from 0.3–0.4 MPa) steady state CoF remains consistent at approximately $\mu \sim 0.03$ (Katta et al., 2007). This studies level of $F_Z$ deviation is unlikely to significantly impact the tribological performance or the general conclusions drawn from the study.

Table 2 also summarises the mean overall strain recovery ($\varepsilon_r$), the mean startup CoF ($\mu_S$, measured at $t = 1800$ s) and the mean final CoF ($\mu_F$, measured at $t = 3600$ s) with one standard deviation of error for all test scenarios detailed in Table 1. Strain recovery ($\varepsilon_r$) was noted for five out of six contact conditions explored during the sliding phase coinciding with decreasing CoF, broadly complying with the principles of IFP theory (Eq. (1)). The only sample that did not exhibit reducing strain or CoF was PEEK - SCA cartilage which is expected, as this configuration facilitates no rehydration mechanism. The specific relationship between CoF and strain recovery for each contact pair are discussed in subsequent sections. Principally, this methodology attempts to replicate the fluid recovery processes inherent to physiological cartilage–cartilage interactions and contrast with the rehydration capabilities of SPMK-g-PEEK (Elkington et al., 2024a, 2023, 2024b).

### 3.1. Effect of contact geometry (SCA vs. cSCA)

Greater cartilage strain recovery ($\varepsilon_r$) and subsequently lower final CoF are expected for cSCA geometry cartilage pins. This geometry facilitates tribological rehydration through hydrodynamic pressurisation in the convergent-wedge inlet, in contrast to SCA, which lacks a convergent wedge and operates independently of tribological rehydration (Moore, 2017; Elkington et al., 2024b). Table 3 summarises the independent *t*-tests performed for each substrate (PEEK, SPMK-g-PEEK, cartilage condyle) interfaced with cartilage in SCA and cSCA conditions. For all contact pairs, the startup CoF ($\mu_S$) is unaffected by contact geometry ($p > 0.7$), which is expected as this corresponds to the cartilage pin is in the highest strain state ahead of any rehydration. Overall strain recovery ($\varepsilon_r$) is enhanced by tribological rehydration (cSCA conditions) against engineered PEEK and SPMK-g-PEEK substrates ($p < 0.05$). Whereas against a cartilage condyle, the contribution of strain recovery attributed to tribological rehydration is reduced ($p = 0.15$), suggesting fluid recovery is dominated by fluid confinement within the interfacial gaps of opposing cartilage surfaces (Wu and Ferguson, 2017; Liao et al., 2019; Putignano et al., 2021). In contrast, for the condyle and SPMK-g-PEEK cases, the contact geometry (SCA versus cSCA) does not significantly impact the final CoF ($\mu_F$, $p > 0.4$), demonstrating in each case the magnitude of fluid recovery was sufficient to recover IFP. Further discussion of statistical significance is provided in subsequent sections alongside the experimental data to delineate specific fluid recovery and tribological mechanisms.

#### 3.1.1. Cartilage vs. Cartilage condyle

Fig. 4 illustrates strain recovery from which fluid recovery is inferred for SCA and cSCA cartilage plugs throughout sliding against a cartilage condyle, indicating the recovery of interstitial fluid. Cartilage condyles sliding against the SCA plug (Fig. 4(a)) exhibited strain recovery of $\varepsilon_r = 8.77 \pm 3.10\%$. A greater strain reduction was observed for the cSCA condition (Fig. 4(b)) of $\varepsilon_r = 14.11 \pm 4.15\%$, though this result is not statistically significant ($p = 0.15$). In both instances the startup CoF at the onset of sliding was approximately $\mu_S \sim 0.13$ ($p = 0.75$), and decreased throughout sliding towards similar final CoF of $\mu_F = 0.049 \pm 0.012$ and $\mu_F = 0.038 \pm 0.020$ for the SCA and cSCA cases respectively ($p = 0.47$). Observation of strain recovery in both instances corresponds to a substantially reduced final CoF ($\mu_F$), broadly complying with IFP theory (Eq. (1)) (Moore et al., 2017; Caligaris and Ateshian, 2008). The authors recognise that the low sample size (N = 3) limits the statistical power of this study. Hence the contribution of tribological rehydration (cSCA condition) to strain recovery is not conclusively elucidated within this experiment, and is indicated by a low non-significant *p*-value ($p = 0.15$). However, the high strain recovery observed in the SCA condition ($\varepsilon_r = 8.77 \pm 3.10\%$), clearly suggests that matched cartilage rehydration appears to be dominated by alternate fluid recovery mechanisms native to interfacing synovial tissue. Potential mechanisms are discussed in later sections (Section 3.2).

The matched cartilage configuration provides a closer approximation to conformal synovial joint mechanics compared to simplified

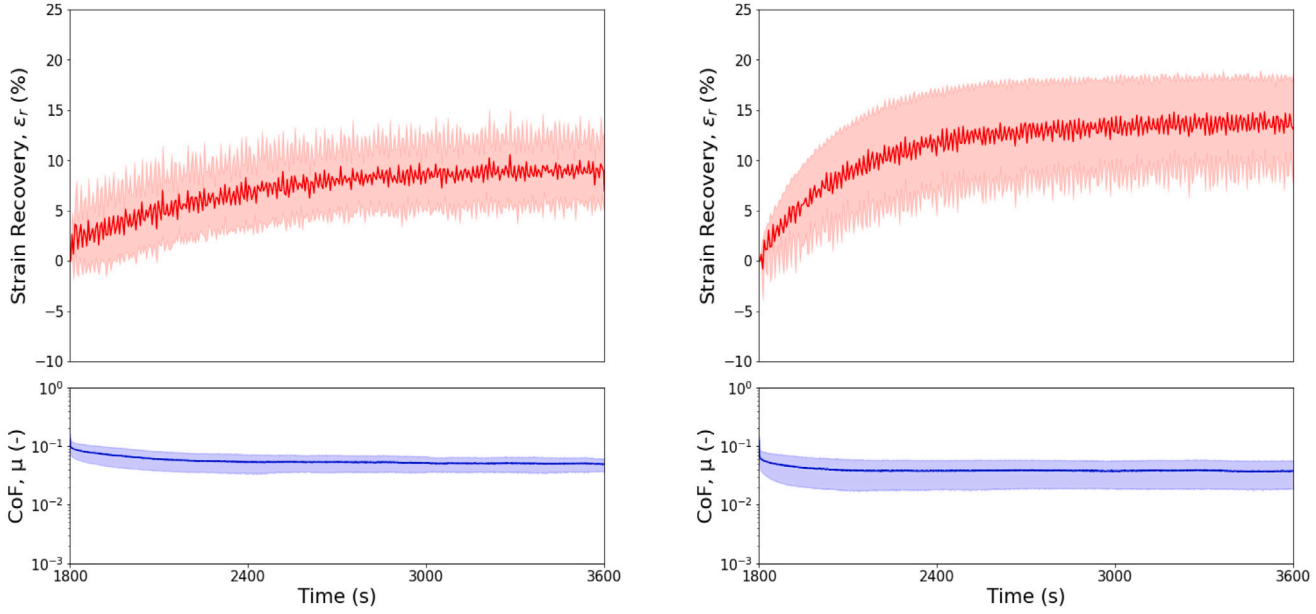


(a) SCA-Condyle (N = 3). (b) cSCA-condyle (N = 3).

**Fig. 4.** Strain recovery ($\varepsilon_r(t)$) and CoF ($\mu(t)$) data for the sliding phase of SCA and cSCA cartilage pins against a bovine condyle.

pin-on-plate studies, while maintaining greater experimental control than conformal hip pendulum setups (Bei and Fregly, 2004). Previous studies on self-mated cartilage, using both human hip pendulum experiments and multiaxial joint simulators, have consistently reported low CoF values between 0.01–0.06, implying sustained IFP for maintaining low friction (Unsworth et al., 1975b,a; McCann et al., 2008). Benchtop pin-on-plate studies of matched cartilage–cartilage contacts also typically examine only CoF, sustained in the region of 0.01–0.05 during ≤ 1 h long testing (Link et al., 2020; Northwood et al., 2007; Katta et al., 2007; Caligaris and Ateshian, 2008). The self-mated cartilage experiments detailed in this study (Fig. 4) demonstrate a CoF ($\mu_F$) of < 0.05, comparable to anticipated values, with the addition of in-situ quantification of strain recovery quantifying reuptake of interstitial fluid.

### 3.1.2. Cartilage vs. PEEK

No strain recovery, indicating no rehydration, was observed for SCA cartilage sliding against PEEK plates (Fig. 5(a)), exhibited as a continuous strain increase throughout sliding ($\varepsilon_r$ = −4.69 ± 1.60%). This observation is consistent with prior research, resembling unconfined compression, within which the flat SCA geometry fails to generate a hydrodynamic pressurisation zone necessary for facilitating fluid recovery in cartilage (Elkington et al., 2023, 2024b; Caligaris and Ateshian, 2008; Moore and Burris, 2017). Contrary to IFP theory (Eq. (1)) and earlier findings that correlate increased strain with higher CoF (Caligaris and Ateshian, 2008; Elkington et al., 2024b). A marginal reduction in CoF during the SCA-PEEK sliding phase was observed, from $\mu_S$ = 0.300 ± 0.045 to $\mu_F$ = 0.269 ± 0.064. Considering the high margin of CoF error, both these results essentially align with the maximal equilibrium CoF for SCA-PEEK (Elkington et al., 2023, 2024b). Indicating that the marginal differences observed are indicative of no effective fluid recovery, and the loss of IFP following compression completely inhibits cartilage lubrication.

The cSCA-PEEK condition (Fig. 5(b)) significantly enhances interstitial fluid recovery ($p$ = 0.003) resulting in a strain recovery of $\varepsilon_r$ = 4.15 ± 1.01%, indicating effective tribological rehydration (Moore and Burris, 2017). Correspondingly, the reduction from a high startup CoF ($\mu_S$ = 0.282 = ± 0.069) to a final CoF ($\mu_F$ = 0.148 ± 0.037) approached significance ($p$ = 0.061). Indicating effective tribological rehydration consistent with IFP theory (Eq. (1)) (Moore and Burris, 2017; Farnham et al., 2021). However, the resultant final CoF, significantly exceeds safe physiological friction levels (∼ $\mu \leq 0.1$) (Moore et al., 2017), suggesting that only partial restoration of IFP was achieved. Comparatively, previous studies of glass interfaced with cSCA cartilage at a lower 7 N load (∼0.2 MPa) demonstrate speeds of 60–80 mm/s are required to achieve sufficient tribological rehydration for sustaining a physiological CoF of < 0.04 (Moore and Burris, 2017; Burris and Moore, 2017; Kupratis et al., 2021), corresponding to a strain recovery of $\varepsilon_r$ ∼ 6% (Kupratis et al., 2021; Farnham et al., 2021). The lower sliding speeds used in this study of 22.1–33.4 mm/s are consistent with the speed threshold for initiating tribological rehydration (Burris and Moore, 2017; Kupratis et al., 2021; Moore and Burris, 2017), with similar studies observing CoF in the range of 0.1–0.3 (Burris and Moore, 2017; Kupratis et al., 2021) and strain recovery of $\varepsilon_r$ ∼ 1% at 30 mm/s (Kupratis et al., 2021). The greater strain recovery of $\varepsilon_r$ = 4.15 ± 1.01% observed herein is attributed to the application of a higher load of 20 N (∼0.50 MPa). This higher load predisposes the cartilage to a greater degree of compression-induced strain, facilitating a more substantial recovery along with increased hydrodynamic pressurisation during sliding, thereby promoting more fluid recovery (Burris and Moore, 2017; Elkington et al., 2024a; Katta et al., 2007).

### 3.1.3. Cartilage vs. SPMK-g-PEEK

Strain recovery indicative of rehydration occurred for both the SCA and cSCA cartilage pins sliding against SPMK-g-PEEK, as shown in Fig. 6. SCA-SPMK (Fig. 6(a)) resulted in a total strain recovery of $\varepsilon_r$ = 7.04 ± 1.71%, and cSCA-SPMK (Fig. 6(b)) exhibited a significantly greater strain recovery of $\varepsilon_r$ = 12.95 ± 2.55% ($p$ = 0.041). Minor discrepancies between low CoF measurements (i.e., ranges below $\mu$ < 0.05) are often attributed to sample misalignment rather than mechanistic differences (Burris and Sawyer, 2009). Therefore respective startup and final CoF for the SCA-SPMK and cSCA-SPMK conditions (Table 2) are considered nominally equivalent and are statistically insignificant. For both contact geometries against the highly lubricious SPMK-g-PEEK surface, the onset of sliding yielded a startup CoF of $\mu_S$ ∼ 0.04 ($p$ = 0.768) before reaching a steady state $\mu_F$ ∼ 0.01 ($p$ = 0.398). Concurrent strain recovery and CoF reduction during the sliding phase suggest compliance with the principles of IFP (Eq. (1)) with increasing fluid load support corresponding to attenuated friction.

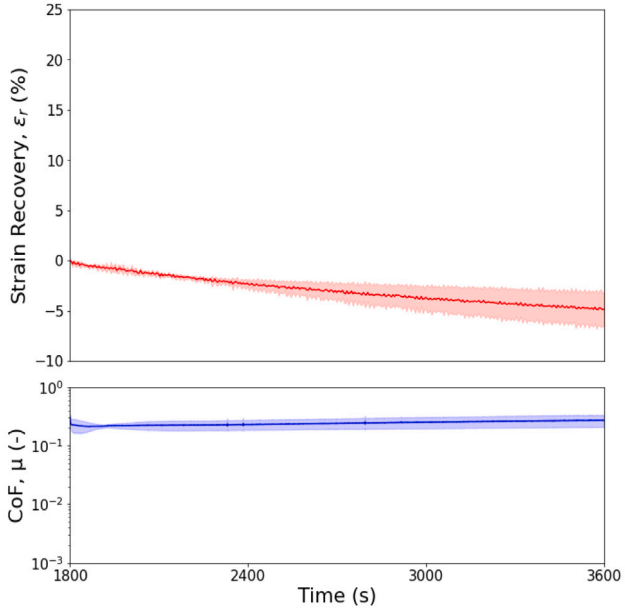


(a) SCA-PEEK (N = 3).

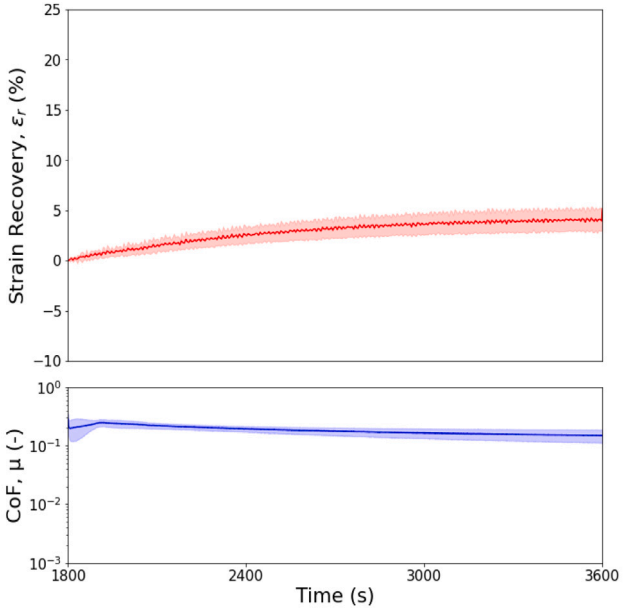


(b) cSCA-PEEK (N = 3).

**Fig. 5.** Strain recovery ($\varepsilon_r(t)$) and CoF ($\mu(t)$) data for the sliding phase of SCA and cSCA cartilage pins against unfunctionalised PEEK.

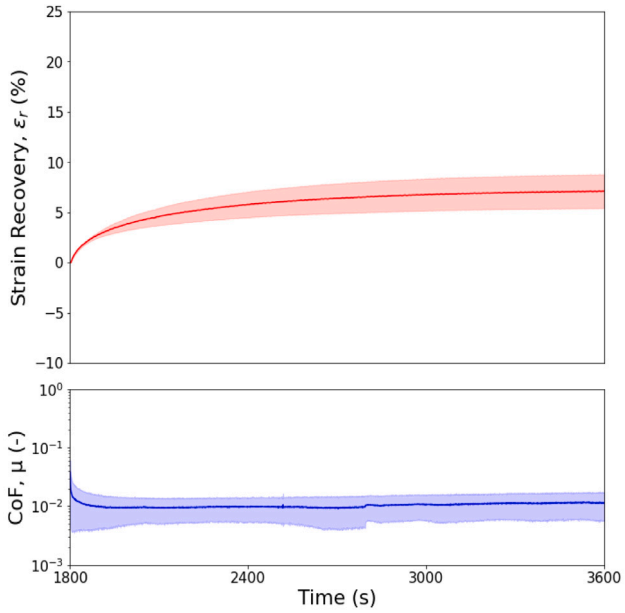


(a) SCA-SPMK (N = 3).

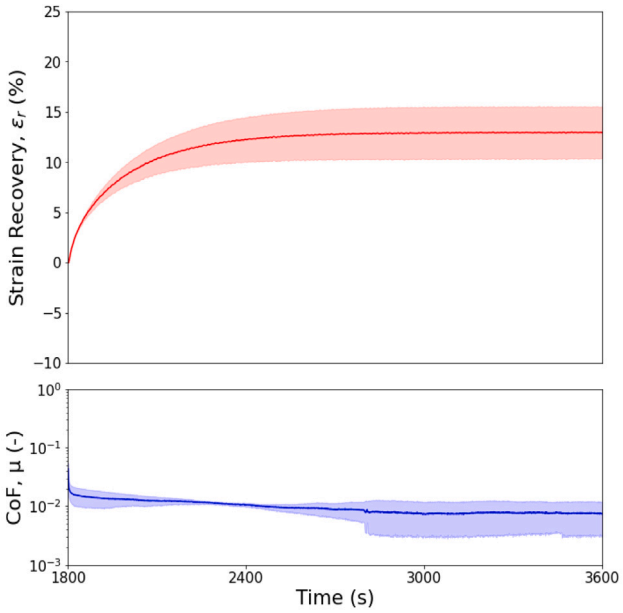


(b) cSCA-SPMK (N = 3).

**Fig. 6.** Strain recovery ($\varepsilon_r(t)$) and CoF ($\mu(t)$) data for the sliding phase of SCA and cSCA cartilage pins against SPMK-g-PEEK.

Demonstration of rehydration ($\varepsilon_r$ = 7.04 ± 1.71%) for the SCA-SPMK interface aligns with previous studies of PETR in the same contact conditions at higher loads of 30 N (~0.75 MPa) at 10 mm/s exhibiting $\varepsilon_r \sim$ 8%–11% (Elkington et al., 2024b,a). The greater overall strain recovery observed for the cSCA-SPMK condition ($\varepsilon_r$ = 12.95 ± 2.55%, $p$ = 0.041), compared to the SCA condition, indicates the mechanisms of PETR and convergent contact tribological rehydration are additive, resulting in an enhanced strain recovery. This provides greater fluid recovery than observations of cSCA tribological rehydration exclusive to convergent wedge effects, as observed against the unfunctionalised PEEK (Fig. 5(b)) and in previous studies (Farnham et al., 2021; Elkington et al., 2024b; Kupratis et al., 2021). Notably, enhanced strain recovery does significantly correspond to reduced final CoF between SCA and cSCA contacts ($\mu_F$, $p$ = 0.398), highlighting

**Table 4**
Substrate effects: Comparison of mean overall strain recovery ($\varepsilon_r$), startup CoF ($\mu_S$) and final CoF ($\mu_F$) between PEEK, SPMK-g-PEEK and matched cartilage substrates for both SCA and cSCA conditions using independent *t*-tests. The *t*-statistic measures the difference between the sample means in terms of standard deviations, and the *p*-value indicates the statistical significance of the observed differences.

| Sample pair | Strain recovery ($\varepsilon_r$) | | Startup CoF ($\mu_S$) | | Final CoF ($\mu_F$) | |
|---|---|---|---|---|---|---|
| | *t*-statistic | *p*-value | *t*-statistic | *p*-value | *t*-statistic | *p*-value |
| SCA-Condyle vs. SCA-PEEK | 6.683 | 0.007 | −5.238 | 0.008 | −5.852 | 0.024 |
| cSCA-Condyle vs. cSCA-PEEK | 4.039 | 0.046 | −3.75 | 0.046 | −4.530 | 0.019 |
| SCA-SPMK vs. SCA-PEEK | 10.433 | 0.001 | −8.898 | 0.003 | −6.952 | 0.019 |
| cSCA-SPMK vs. cSCA-PEEK | 5.557 | 0.016 | −5.911 | 0.024 | −6.562 | 0.021 |
| SCA-Condyle vs. SCA-SPMK | 0.910 | 0.442 | 4.114 | 0.017 | 4.906 | 0.017 |
| cSCA-Condyle vs. cSCA-SPMK | 0.412 | 0.705 | 5.122 | 0.016 | 2.633 | 0.110 |

that the aqueous lubrication of SPMK-g-PEEK substantially influences cartilage friction.

The SPMK-g-PEEK surface introduces a highly hydrated polyelectrolyte interface, providing effective aqueous boundary lubrication. Previous studies have shown that lubricity of SPMK-g-PEEK is independent of speed, maintaining constant low CoF (< 0.02) across a speed range of 1–200 mm/s up to 1.2 MPa contact pressures against cartilage (Elkington et al., 2024a). The inherent lubricity of the SPMK-g-PEEK interface facilitates low CoF even after compressive cartilage dehydration, with both SCA and cSCA contacts exhibiting a startup CoF of $\mu_S \sim 0.04$. The SPMK-g-PEEK startup CoF observed within this study is marginally higher than previous studies ($\mu_S < 0.02$, sliding speed = 10 mm/s) (Elkington et al., 2024b). Whilst this discrepancy maybe be attributed experimental hardware differences in sample alignment (Burris and Sawyer, 2009), greater shear forces resulting from higher sliding speeds likely increase friction in cartilage following compression, where rehydration has not yet occurred to supplement fluid load support.

### 3.2. Substrate effects

Table 4 summarises the independent *t*-tests performed for each cartilage contact geometry condition (SCA, cSCA) interfaced with each substrate (PEEK, SPMK, cartilage condyle). Aside from tribological rehydration afforded by a cSCA cartilage geometry, there are clear indications of rehydration attributed to substrate effects. Comparing cartilage condyle and PEEK substrates in both SCA and cSCA configurations, demonstrated significantly greater overall strain recovery ($\varepsilon_r$, $p < 0.05$), lower startup CoF ($\mu_S$, $p < 0.05$), and lower final CoF ($\mu_F$, $p < 0.03$) for cartilage condyle surfaces. The greater overall strain recovery and low friction of matched cartilage is attributed to the increased availability of water in the contact area, as both cartilage can exude water interstitial water and support biphasic fluid–structure interactions to promote rehydration and lubrication (Shim et al., 2021; Hou et al., 1989). Furthermore, compliance of low-modulus matched cartilage contacts promote uniform distribution of contact pressures (Pawaskar et al., 2010; Willing et al., 2014), which may support fluid film lubrication (Hou et al., 1989; Schwartz and Bahadur, 2007). Synovial rehydration mechanisms can be attributed to fluid exchange within the contact gap (Wu and Ferguson, 2017; Liao et al., 2019) and osmotic swelling (Voinier et al., 2022), both of which rely on transient loading within the contact area during sliding, supported by the high compliance distributing contact pressures and roughness of cartilage (i.e. fluid confinement between asperities). However, this study does not isolate specific contributions of synovial tissue rehydration mechanisms, focusing instead on the overall performance of matched cartilage. Conversely, hard biomaterials such as PEEK result in higher contact pressures and comparatively smaller contact areas, resulting in accelerated fluid exudation and higher shear forces (Berkmortel et al., 2020; Khayat, 2015; Willing et al., 2014). Cartilage rehydration and aqueous lubrication are reduced as PEEK surfaces do not provide a hydrated, porous, compliant counterface necessary for effective fluid exchange within the contact area (Elkington et al., 2023). The same trend is observed when comparing SPMK-g-PEEK and PEEK substrates in both SCA and cSCA configurations (Table 4), demonstrating significantly greater overall strain recovery ($\varepsilon_r$, $p < 0.02$), lower startup CoF ($\mu_S$, $p < 0.01$), and lower final CoF ($\mu_F$, $p < 0.02$) for SPMK-g-PEEK substrates. Prior studies measure the SPMK swollen surface height of 5 μm and low modulus of ~500 Pa, indicating a hydrated, cushioning interface that enhances fluid pressurisation within cartilage asperity gaps to facilitate rehydration (Elkington et al., 2024a). Hydrophilic SPMK-g-PEEK counterfaces facilitate aqueous lubrication (low $\mu_S$ and $\mu_F$) and an aqueous reservoir to support cartilage interstitial fluid recovery (high $\varepsilon_r$) through PETR (Elkington et al., 2024a, 2023, 2024b).

Table 4 shows strain recovery promoted by SPMK-g-PEEK substrates attributed to PETR, and strain recovery promoted by condyle substrate attributed to synovial rehydration mechanisms are comparable in both SCA ($\varepsilon_r$, $p = 0.442$) and cSCA conditions ($\varepsilon_r$, $p = 0.705$). The greatest strain recovery was observed in the cSCA condition, with cSCA-SPMK exhibiting $\varepsilon_r = 12.95 \pm 2.55\%$, and cSCA-Condyle exhibiting $\varepsilon_r = 14.11 \pm 4.15\%$ ($p = 0.705$). Providing an initial empirical demonstration that SPMK-g-PEEK can effectively mimic synovial rehydration mechanisms. However, there are distinct differences in lubrication mechanisms. In both SCA and cSCA conditions, SPMK-g-PEEK surfaces exhibit a significantly lower startup CoF ($\mu_S \sim 0.04$) compared to the high startup CoF ($\mu_S \sim 0.13$) observed for cartilage condyles ($p < 0.02$). IFP recovery and enhanced fluid load support, indicated by strain recovery, results in lower final CoF for SPMK-g-PEEK ($\mu_F \sim 0.01$) and condyle ($\mu_F \sim 0.05$) surfaces. Comparing respective contact geometries, there is a statistically greater reduction of final CoF for SCA conditions ($p = 0.02$) than for cSCA conditions ($p = 0.11$). Which is attributed to the greater contribution of tribological rehydration observed for the cSCA-SPMK condition (Table 3). As discussed previously, the lubrication performance of SPMK-g-PEEK is largely independent of IFP, as the high hydration of the surface tethered SPMK polyelectrolyte provides unabating aqueous lubrication (Elkington et al., 2024a, 2023, 2024b). Notably, the startup CoF observed for SPMK-g-PEEK surfaces ($\mu_S \sim 0.04$) is similar in magnitude to the final CoF for matched cartilage condyles ($\mu_F \sim 0.05$). Demonstrating that the lubrication performance of SPMK-g-PEEK can replicate physiological CoF even in contact conditions following compressive fluid exudation with reduced cartilage IFP (Fig. 6). Conversely, lubrication of matched cartilage relies on IFP (Caligaris and Ateshian, 2008), and hence is dependent on strain recovery to restore IFP (Fig. 4).

### 3.3. Clinical significance

Current use of hard biomaterials (e.g. Cobalt-Chromium-Molybdenum) for focal joint repair or hemiarthroplasty compromise fluid-pressure dependent load support of interfacing cartilage, leading to high friction and cartilage erosion (Pawaskar et al., 2011; Diermeier et al., 2020). Indicating that these biomaterials do not facilitate the

sustainable, competitive rehydration essential for supporting healthy cartilage biomechanics (Rossetti, 2022; Guilak et al., 2001). In contrast, matched cartilage surfaces provide a continuous pathway for fluid exchange, supporting hydraulic permeability and osmotic rehydration (Pawaskar et al., 2010). Cartilage fluid recovery to counteract compressive exudation holds significant physiological relevance. Foremost rehydration is required for sustaining IFP and CoF < 0.1 (Moore and Burris, 2017; Moore et al., 2017; Caligaris and Ateshian, 2008), above which can lead to wear of cartilage and pathogenesis of osteoarthritis (Neu et al., 2010; Oungoulian et al., 2015; Chan et al., 2011). Additionally rehydration underpins biological functions (i.e. solute transport and cellular mechanotransduction) (Graham et al., 2017; Schätti et al., 2016; Albro et al., 2008) with observations that activity can prevent osteoarthritis (Williams, 2013) or joint space narrowing by reversing cartilage dehydration due to inactivity (Ekholm and Be, 1952; Ingelmark and Ekholm, 1948).

This study demonstrates interfacing hard biomaterials, such as PEEK (Fig. 5), against cartilage results in vastly reduced strain recovery and higher CoF, highlighting the inadequacy of hard biomaterials in supporting cartilage lubrication and rehydration (Elkington et al., 2023, 2024b). Whereas, friction and interstitial fluid recovery of cartilage is significantly influenced by the surface hydration of opposing cartilage (condyle substrates) or polyelectrolytes (SPMK-g-PEEK substrates) (Caligaris and Ateshian, 2008; Elkington et al., 2024a; Murakami et al., 1999). Compared to PEEK in the SCA condition, cartilage condyle interfaces result in enhanced strain recovery ($\varepsilon_r$ = 8.77 ± 3.10%, $p$ = 0.007) resulting in a substantially lower final CoF ($\mu_F$ = 0.049 ± 0.012, $p$ = 0.024). Similarly SPMK-g-PEEK in the SCA condition, compared to PEEK, results in enhanced strain recovery ($\varepsilon_r$ = 7.04 ± 1.71%, $p$ = 0.001) and a substantially lower CoF ($\mu_F$ = 0.011 ± 0.006, $p$ = 0.019). The SCA condition operates independently of tribological rehydration (Moore and Burris, 2017; Elkington et al., 2024b), and therefore isolates the contributions of each substrate. The contribution of tribological rehydration enhanced overall strain recovery for all substrates (Table 2). Correspondingly, the greatest strain recovery in this dataset was observed for the cSCA-SPMK ($\varepsilon_r$ = 12.95 ± 2.55%) and cSCA-Condyle ($\varepsilon_r$ = 14.11 ± 4.15%) experiments. A key finding of this study is that PETR by SPMK-g-PEEK substrates can reproduce comparable levels matched cartilage (condyle) synovial rehydration, demonstrated by the insignificant strain recovery ($\varepsilon_r$) $p$-values comparing both SCA, $p$ = 0.442, and cSCA conditions, $p$ = 0.705 (Table 4). Furthermore, the superior aqueous lubrication properties of SPMK-g-PEEK are able to facilitate physiological CoF levels at the start of sliding ($\mu_S \sim 0.04$) (Caligaris and Ateshian, 2008; Moore et al., 2017), where cartilage IFP is diminished, contrasting to the higher startup CoF observed for cartilage condyle surfaces ($\mu_S \sim 0.13$). These results confer SPMK-g-PEEK as a compelling biomimetic interface for facilitating cartilage rehydration, and therefore the biological function of cartilage (Graham et al., 2017), and also facilitate low friction comparable to the final CoF of matched cartilage interfaces following effective rehydration and IFP recovery ($\mu_F \sim 0.05$, Fig. 4). Previous studies of low cartilage friction afforded by SPMK-g-PEEK interfaces have been demonstrated to substantially mitigate cartilage wear compared to unfunctionalised biomaterials (Elkington et al., 2023) and facilitate low CoF of damaged cartilage (Elkington et al., 2024b).

Present literature on high water content materials for cartilage resurfacing, hydrogels or polymer brush interfaces, often only consider CoF to evaluate performance against impermeable counterfaces (e.g. glass) (Milner et al., 2018; Pan et al., 2007; Freeman et al., 2000; Blum and Ovaert, 2013; Chen et al., 2017; Baykal et al., 2013; Murakami et al., 2015) or cartilage explants (Kyomoto et al., 2010; Li et al., 2016, 2010). These approaches fail to directly measure the materials' ability to regulate cartilage interstitial fluid recovery. The inference of sustained hydration is often indirectly made through observations of maintained physiological CoF levels, leveraging the understanding of the biphasic nature of these materials (Baykal et al., 2013; Murakami et al., 2015). However, the reliance on CoF as a sole performance indicator may be misleading, posing the risk that materials exhibiting low CoF due to aqueous lubrication alone may not adequately support fluid transport requisite for maintaining cartilage health (Graham et al., 2017). SPMK-g-PEEK is an example of a material that facilitates physiological low cartilage CoF, irrespective of cartilage IFP (Elkington et al., 2024b,a), which is demonstrated by the low CoF observed for cartilage interfaced with SPMK-g-PEEK at the onset of sliding ($\mu_S \sim 0.04$, Fig. 6). The specific PETR mechanism underpinning cartilage strain recovery interfaced with SPMK-g-PEEK has been explicated in a previous study (Elkington et al., 2024a). However future studies of alternate hydrated materials for articulating against cartilage (e.g. hydrogels) should employ studies which evaluate the materials capacity for facilitating cartilage rehydration.

### 3.4. Limitations

The statistical power of this study is constrained by the small sample size (N = 3), providing only an initial indication of SPMK-g-PEEK's efficacy in replicating the fluid exchange and tribological properties of matched articular cartilage. *In vitro* analysis of cartilage tribology inherently faces uncertainties due to the variability in tissue quality and geometry (Moore et al., 2017). The most significant errors were observed in the matched cartilage contacts (Fig. 4), with a strain standard deviation of approximately 3%–4%. In contrast, previous studies on SCA cartilage strain against PEEK substrates reported standard deviations around 2% (Elkington et al., 2024b). The higher standard deviation in matched cartilage contacts is attributed to the compliance of both mated cartilage surfaces, which leads to greater temporal variation in compressive strain. These errors are further compounded by the low sample size. Specifically, this study did not reliably quantify the synergistic effects of cSCA tribological rehydration and synovial rehydration (e.g. osmotic swelling). Future studies should incorporate a larger sample size and aim to optimise the Fuzzy-PI feedback parameters to enhance feedback rate and improve load control.

The development of a tribometer designed to replicate matched cartilage interactions has introduced challenges in accurately measuring contact area or strain under zero interstitial pressure. Additionally, the experiments involving matched cartilage (condyle) and SPMK-g-PEEK interfaces did not strictly adhere to the numerical predictions of IFP theory (Eq. (1)), likely due to additional friction dissipation mechanisms beyond biphasic theory (i.e. aqueous boundary lubrication). To fully elucidate the temporal biomechanical behaviour of cartilage interfaced with candidate biomaterials, future studies should incorporate accurate calculations of interstitial fluid flow using porohyperelastic (De Boer et al., 2020) or multiscale lubrication models (Putignano et al., 2021), alongside detailed experimental analyses.

The influence of dynamic physiological loading, such as gait, on cartilage tribology and fluid pressurisation remains debated in the literature (Sadeghi et al., 2015; Krishnan et al., 2005). This study focused on constant loading at 20 N. Future investigations using the Fuzzy-PI tribometer (Fig. 2) will examine the effects of variable loading and physiological velocity profiles on cartilage–cartilage tribological rehydration and assess the ability of SPMK-g-PEEK to replicate this behaviour under physiological duty cycles. Furthermore, this dynamically responsive *in vitro* apparatus and associated techniques could feasibly be employed for validating other soft viscoelastic materials for tissue and cartilage repair (Nayar et al., 2012; Erdemir et al., 2015).

## 4. Conclusions

This study demonstrates the efficacy of SPMK-g-PEEK as a biomi metic material for focal cartilage repair, capable of facilitating sustained low friction and interstitial fluid recovery comparable to matched

cartilage–cartilage interfaces. The development of a Fuzzy-PI controlled biotribometer for *in vitro* assessment of cartilage contact models facilitated concurrent measurement of friction and strain recovery attributable to interstitial fluid maintenance. Through a dual-phase testing approach, encompassing compression and subsequent compression-sliding, this methodology permits direct quantification of cartilage's interstitial fluid recovery after static exudation phases, revealing rehydration dynamics.

Our results demonstrate the rehydration of matched cartilage contacts with fluid exchange attributable to osmotic swelling and hydrodynamic tribological rehydration, establishing a physiological benchmark for strain recovery ($\varepsilon_r \sim 14\%$) and low friction ($\mu \sim 0.04$) following a period of compressive cartilage dehydration. In contrast, PEEK surfaces hinder fluid influx, leading to high CoF and limited interstitial fluid recovery during sliding. SPMK-g-PEEK surfaces, with an engineered polyelectrolyte-enhanced tribological rehydration mechanism, exhibited comparable tribological behaviour to matched cartilage contacts, resulting in strain recovery of $\varepsilon_r \sim 13\%$ and lower friction, $\mu \sim 0.01$. This highlights the effectiveness of SPMK-g-PEEK in maintaining near-surface hydration, which is synonymous with cartilage lubrication and rehydration, offering inherent advantages over currently employed hard biomaterials used in cartilage repair. Overall, SPMK-g-PEEK presents a promising biomimetic solution for cartilage repair, effectively mimicking the natural rehydration and lubrication mechanisms essential for joint health and longevity.

## CRediT authorship contribution statement

**Robert J. Elkington:** Writing – review & editing, Writing – original draft, Visualization, Validation, Software, Resources, Methodology, Investigation, Formal analysis, Data curation, Conceptualization. **Gregory M. Pryce:** Software, Methodology, Investigation, Data curation, Conceptualization. **David Keeling:** Software, Resources. **Richard M. Hall:** Supervision, Data Analysis. **Andrew R. Beadling:** Writing – review & editing, Supervision. **Hemant Pandit:** Supervision, Funding acquisition. **Michael G. Bryant:** Writing – review & editing, Supervision, Resources, Project administration, Funding acquisition, Conceptualization.

## Creative commons

For the purpose of open access, the author has applied a Creative Commons Attribution (CC BY) licence to any Author Accepted Manuscript version arising from this submission.

## Declaration of competing interest

The authors declare that they have no known competing financial interests or personal relationships that could have appeared to influence the work reported in this paper.

## Acknowledgments

Funding for this project was received from the UKRI Engineering and Physical Sciences Research Council.

The authors acknowledge the support and funding of the Bragg Centre for Materials Research at the University of Leeds (No. 2441039).

The authors acknowledge the support and funding of Friction: The Tribology Enigma which is funded by the Engineering and Physical Sciences Research Council, United Kingdom, under grant no. EP/R001 766/1.

## Appendix A. Supplementary data

Supplementary material related to this article can be found online at https://doi.org/10.1016/j.jmbbm.2025.106964.

## Data availability

Data will be made available on request.

## References

Accardi, M.A., Dini, D., Cann, P.M., 2011. Experimental and numerical investigation of the behaviour of articular cartilage under shear loading—interstitial fluid pressurisation and lubrication mechanisms. Tribol. Int. 44 (5), 565–578.

Albro, M.B., Chahine, N.O., Li, R., Yeager, K., Hung, C.T., Ateshian, G.A., 2008. Dynamic loading of deformable porous media can induce active solute transport. J. Biomech. 41 (15), 3152–3157.

Ateshian, G.A., 2009. The role of interstitial fluid pressurization in articular cartilage lubrication. J. Biomech. 42 (9), 1163–1176.

Baykal, D., Underwood, R., Mansmann, K., Marcolongo, M., Kurtz, S., 2013. Evaluation of friction properties of hydrogels based on a biphasic cartilage model. J. Mech. Behav. Biomed. Mater. 28, 263–273.

Bei, Y., Fregly, B.J., 2004. Multibody dynamic simulation of knee contact mechanics. Med. Eng. Phys. 26 (9), 777–789.

Bell, C., Ingham, E., Fisher, J., 2006. Influence of hyaluronic acid on the time-dependent friction response of articular cartilage under different conditions. Proc. Inst. Mech. Eng. H: J. Eng. Med. 220 (1), 23–31.

Berkmortel, C., Langohr, G.D.G., King, G., Johnson, J., 2020. Hemiarthroplasty implants should have very low stiffness to optimize cartilage contact stress. J. Orthop. Res.® 38 (8), 1719–1726.

Blum, M.M., Ovaert, T.C., 2013. Low friction hydrogel for articular cartilage repair: evaluation of mechanical and tribological properties in comparison with natural cartilage tissue. Mater. Sci. Eng.: C 33 (7), 4377–4383.

Brand, R.A., 2005. Joint contact stress: a reasonable surrogate for biological processes? Iowa Orthop. J. 25, 82.

Brittberg, M., Gomoll, A.H., Canseco, J.A., Far, J., Lind, M., Hui, J., 2016. Cartilage repair in the degenerative ageing knee: a narrative review and analysis. Acta Orthop. 87 (sup363), 26–38.

Burris, D.L., Moore, A.C., 2017. Cartilage and joint lubrication: new insights into the role of hydrodynamics. Biotribology 12, 8–14.

Burris, D., Sawyer, W., 2009. Addressing practical challenges of low friction coefficient measurements. Tribol. Lett. 35, 17–23.

Caligaris, M., Ateshian, G.A., 2008. Effects of sustained interstitial fluid pressurization under migrating contact area, and boundary lubrication by synovial fluid, on cartilage friction. Osteoarthr. Cartil. 16 (10), 1220–1227.

Cederlund, A.A., Aspden, R.M., 2022. Walking on water: revisiting the role of water in articular cartilage biomechanics in relation to tissue engineering and regenerative medicine. J. R. Soc. Interface 19 (193), 20220364.

Chan, S., Neu, C., Komvopoulos, K., Reddi, A., Di Cesare, P., 2011. Friction and wear of hemiarthroplasty biomaterials in reciprocating sliding contact with articular cartilage.

Chen, K., Yang, X., Zhang, D., Xu, L., Zhang, X., Wang, Q., 2017. Biotribology behavior and fluid load support of PVA/HA composite hydrogel as artificial cartilage. Wear 376, 329–336.

Cooper, C., Snow, S., McAlindon, T.E., Kellingray, S., Stuart, B., Coggon, D., Dieppe, P.A., 2000. Risk factors for the incidence and progression of radiographic knee osteoarthritis. Arthritis Rheum.: Off. J. Am. Coll. Rheumatol. 43 (5), 995–1000.

Cutcliffe, H.C., Davis, K.M., Spritzer, C.E., DeFrate, L., 2020. The characteristic recovery time as a novel, noninvasive metric for assessing in vivo cartilage mechanical function. Ann. Biomed. Eng. 48, 2901–2910.

Dabiri, Y., Li, L., 2015. Focal cartilage defect compromises fluid-pressure dependent load support in the knee joint. Int. J. Numer. Methods Biomed. Eng. 31 (6), e02713.

De Boer, G., Raske, N., Soltanahmadi, S., Dowson, D., Bryant, M., Hewson, R., 2020. A porohyperelastic lubrication model for articular cartilage in the natural synovial joint. Tribol. Int. 149, 105760.

Diermeier, T., Venjakob, A., Byrne, K., Burgkart, R., Foehr, P., Milz, S., Imhoff, A.B., Vogt, S., 2020. Effects of focal metallic implants on opposing cartilage–an in-vitro study with an abrasion test machine. BMC Musculoskelet. Disord. 21 (1), 1–7.

Eckstein, F., Tieschky, M., Faber, S., Englmeier, K.-H., Reiser, M., 1999. Functional analysis of articular cartilage deformation, recovery, and fluid flow following dynamic exercise in vivo. Anat. Embryol. (Berl). 200, 419–424.

Ekholm, R., Be, I., 1952. Functional thickness variations of human articular cartilage.. Acta Soc. Medicorum Ups. 57 (1–2), 39–59.

Elkington, R.J., Hall, R.M., Beadling, A.R., Pandit, H., Bryant, M.G., 2023. Highly lubricious SPMK-g-PEEK implant surfaces to facilitate rehydration of articular cartilage. J. Mech. Behav. Biomed. Mater. 147, 106084.

Elkington, R.J., Hall, R.M., Beadling, A.R., Pandit, H., Bryant, M.G., 2024a. Brushing up on cartilage lubrication: Polyelectrolyte enhanced tribological rehydration. Prepr. Submitt. Langmuir.

Elkington, R.J., Hall, R.M., Beadling, A.R., Pandit, H., Bryant, M.G., 2024b. Engineering tribological rehydration of cartilage interfaces: assessment of potential polyelectrolyte mechanisms. Tribol. Int..

Erdemir, A., Bennetts, C., Davis, S., Reddy, A., Sibole, S., 2015. Multiscale cartilage biomechanics: technical challenges in realizing a high-throughput modelling and simulation workflow. Interface Focus. 5 (2), 20140081.

Espinosa, M.G., Otarola, G.A., Hu, J.C., Athanasiou, K.A., 2021. Cartilage assessment requires a surface characterization protocol: roughness, friction, and function. Tissue Eng. C: Methods 27 (4), 276–286.

Farnham, M.S., Ortved, K.F., Horner, J.S., Wagner, N.J., Burris, D.L., Price, C., 2021. Lubricant effects on articular cartilage sliding biomechanics under physiological fluid load support. Tribol. Lett. 69, 1–14.

Fife, R.S., Brandt, K.D., Braunstein, E.M., Katz, B.P., Shelbourne, K.D., Kalasinski, L.A., Ryan, S., 1991. Relationship between arthroscopic evidence of cartilage damage and radiographic evidence of joint space narrowing in early osteoarthritis of the knee. Arthritis Rheum.: Off. J. Am. Coll. Rheumatol. 34 (4), 377–382.

Forster, H., Fisher, J., 1996. The influence of loading time and lubricant on the friction of articular cartilage. Proc. Inst. Mech. Eng. H: J. Eng. Med. 210 (2), 109–119.

Forster, H., Fisher, J., 1999. The influence of continuous sliding and subsequent surface wear on the friction of articular cartilage. Proc. Inst. Mech. Eng. H: J. Eng. Med. 213 (4), 329–345.

Freeman, M.E., Furey, M.J., Love, B.J., Hampton, J.M., 2000. Friction, wear, and lubrication of hydrogels as synthetic articular cartilage. Wear 241 (2), 129–135.

Graham, B.T., Moore, A.C., Burris, D.L., Price, C., 2017. Sliding enhances fluid and solute transport into buried articular cartilage contacts. Osteoarthr. Cartil. 25 (12), 2100–2107.

Guilak, F., Butler, D.L., Goldstein, S.A., 2001. Functional tissue engineering: the role of biomechanics in articular cartilage repair. Clin. Orthop. Relat. Res.® 391, S295–S305.

Henderson, C.E., Higginson, J.S., Barrance, P.J., 2011. Comparison of MRI-based estimates of articular cartilage contact area in the tibiofemoral joint.

Herberhold, C., Faber, S., Stammberger, T., Steinlechner, M., Putz, R., Englmeier, K., Reiser, M., Eckstein, F., 1999. In situ measurement of articular cartilage deformation in intact femoropatellar joints under static loading. J. Biomech. 32 (12), 1287–1295.

Hinterwimmer, S., Gotthardt, M., von Eisenhart-Rothe, R., Sauerland, S., Siebert, M., Vogl, T., Eckstein, F., Graichen, H., 2005. In vivo contact areas of the knee in patients with patellar subluxation. J. Biomech. 38 (10), 2095–2101.

Hou, J., Holmes, M., Lai, W., Mow, V., 1989. Boundary conditions at the cartilage-synovial fluid interface for joint lubrication and theoretical verifications. J. Biomech. Eng..

Ingelmark, B., Ekholm, R., 1948. A study on variations in the thickness of articular cartilage in association with rest and periodical load; an experimental investigation on rabbits. Upsala Lakareforenings Förh. 53 (1–2), 61–74.

Iyer, K.R., Keeling, D., Hall, R.M., 2024. A novel and advanced control method based on fuzzy-PI for joint wear simulators. Open Res. Eur. 4 (6), 6.

Jermin, P., Yates, J., McNicholas, M., 2015. (Vi) focal resurfacing implants in the knee and partial knee replacements. Orthop. Trauma 29 (1), 38–47.

Jeuken, R.M., van Hugten, P.P., Roth, A.K., Timur, U.T., Boymans, T.A., van Rhijn, L.W., Bugbee, W.D., Emans, P.J., 2021. A systematic review of focal cartilage defect treatments in middle-aged versus younger patients. Orthop. J. Sport. Med. 9 (10), 23259671211031244.

Katta, J., Pawaskar, S., Jin, Z., Ingham, E., Fisher, J., 2007. Effect of load variation on the friction properties of articular cartilage. Proc. Inst. Mech. Eng. J: J. Eng. Tribol. 221 (3), 175–181.

Khayat, A., 2015. Effect of Hemiarthroplasty Implant Contact Geometry and Material on Early Cartilage Wear. The University of Western Ontario (Canada).

Krishnan, R., Kopacz, M., Ateshian, G.A., 2004. Experimental verification of the role of interstitial fluid pressurization in cartilage lubrication. J. Orthop. Res. 22 (3), 565–570.

Krishnan, R., Mariner, E.N., Ateshian, G.A., 2005. Effect of dynamic loading on the frictional response of bovine articular cartilage. J. Biomech. 38 (8), 1665–1673.

Kupratis, M.E., Gure, A.E., Ortved, K.F., Burris, D.L., Price, C., 2021. Comparative tribology: articulation-induced rehydration of cartilage across species. Biotribology 25, 100159.

Kurtz, S.M., Lau, E., Ong, K., Zhao, K., Kelly, M., Bozic, K.J., 2009. Future young patient demand for primary and revision joint replacement: national projections from 2010 to 2030. Clin. Orthop. Relat. Res.® 467, 2606–2612.

Kyomoto, M., Moro, T., Saiga, K.-i., Miyaji, F., Kawaguchi, H., Takatori, Y., Nakamura, K., Ishihara, K., 2010. Lubricity and stability of poly (2-methacryloyloxyethyl phosphorylcholine) polymer layer on Co–Cr–Mo surface for hemi-arthroplasty to prevent degeneration of articular cartilage. Biomater. 31 (4), 658–668.

Li, F., Su, Y., Wang, J., Wu, G., Wang, C., 2010. Influence of dynamic load on friction behavior of human articular cartilage, stainless steel and polyvinyl alcohol hydrogel as artificial cartilage. J. Mater. Sci., Mater. Med. 21, 147–154.

Li, F., Wang, A., Wang, C., 2016. Analysis of friction between articular cartilage and polyvinyl alcohol hydrogel artificial cartilage. J. Mater. Sci., Mater. Med. 27, 1–8.

Liao, J., Smith, D.W., Miramini, S., Thibbotuwawa, N., Gardiner, B.S., Zhang, L., 2019. The investigation of fluid flow in cartilage contact gap. J. Mech. Behav. Biomed. Mater. 95, 153–164.

Lin, W., Klein, J., 2021. Recent progress in cartilage lubrication. Adv. Mater. 33 (18), 2005513.

Link, J.M., Salinas, E.Y., Hu, J.C., Athanasiou, K.A., 2020. The tribology of cartilage: Mechanisms, experimental techniques, and relevance to translational tissue engineering. Clin. Biomech. 79, 104880.

Linn, F.C., 1967. Lubrication of animal joints: I. The arthrotripsometer. JBJS 49 (6), 1079–1098.

Liu, Y., Zhou, G., Cao, Y., 2017. Recent progress in cartilage tissue engineering—our experience and future directions. Eng. 3 (1), 28–35.

Maiese, K., 2016. Picking a bone with WISP1 (CCN4): new strategies against degenerative joint disease. J. Transl. Sci. 1 (3), 83.

Makris, E.A., Gomoll, A.H., Malizos, K.N., Hu, J.C., Athanasiou, K.A., 2015. Repair and tissue engineering techniques for articular cartilage. Nat. Rev. Rheumatol. 11 (1), 21–34.

Mastbergen, S.C., Saris, D.B., Lafeber, F.P., 2013. Functional articular cartilage repair: here, near, or is the best approach not yet clear? Nat. Rev. Rheumatol. 9 (5), 277–290.

McCann, L., Udofia, I., Graindorge, S., Ingham, E., Jin, Z., Fisher, J., 2008. Tribological testing of articular cartilage of the medial compartment of the knee using a friction simulator. Tribol. Int. 41 (11), 1126–1133.

McCutchen, C.W., 1962. The frictional properties of animal joints. Wear 5 (1), 1–17.

Merkher, Y., Sivan, S., Etsion, I., Maroudas, A., Halperin, G., Yosef, A., 2006. A rational human joint friction test using a human cartilage-on-cartilage arrangement. Tribol. Lett. 22, 29–36.

Milner, P.E., Parkes, M., Puetzer, J.L., Chapman, R., Stevens, M.M., Cann, P., Jeffers, J.R., 2018. A low friction, biphasic and boundary lubricating hydrogel for cartilage replacement. Acta Biomater. 65, 102–111.

Moore, A.C., 2017. Independent and Competing Roles of Fluid Exudation and Rehydration in Cartilage Mechanics and Tribology. University of Delaware.

Moore, A.C., Burris, D.L., 2015. Tribological and material properties for cartilage of and throughout the bovine stifle: support for the altered joint kinematics hypothesis of osteoarthritis. Osteoarthr. Cartil. 23 (1), 161–169.

Moore, A.C., Burris, D.L., 2017. Tribological rehydration of cartilage and its potential role in preserving joint health. Osteoarthr. Cartil. 25 (1), 99–107.

Moore, A.C., Schrader, J.L., Ulvila, J.J., Burris, D.L., 2017. A review of methods to study hydration effects on cartilage friction. Tribol.- Mater. Surf. Interfaces 11 (4), 202–214.

Murakami, T., Sawae, Y., Horimoto, M., Noda, M., 1999. Role of surface layers of natural and artificial cartilage in thin film lubrication. In: Tribology Series. Vol. 36, Elsevier, pp. 737–747.

Murakami, T., Yarimitsu, S., Nakashima, K., Sakai, N., Yamaguchi, T., Sawae, Y., Suzuki, A., 2015. Biphasic and boundary lubrication mechanisms in artificial hydrogel cartilage: A review. Proc. Inst. Mech. Eng. H: J. Eng. Med. 229 (12), 864–878.

Nayar, V.T., Weiland, J.D., Hodge, A.M., 2012. Macrocompression and nanoindentation of soft viscoelastic biological materials. Tissue Eng. C: Methods 18 (12), 968–975.

Neu, C., Reddi, A., Komvopoulos, K., Schmid, T., Di Cesare, P., 2010. Increased friction coefficient and superficial zone protein expression in patients with advanced osteoarthritis. Arthritis Rheum. 62 (9), 2680–2687.

Northwood, E., Fisher, J., Kowalski, R., 2007. Investigation of the friction and surface degradation of innovative chondroplasty materials against articular cartilage. Proc. Inst. Mech. Eng. H: J. Eng. Med. 221 (3), 263–279.

Oungoulian, S.R., Durney, K.M., Jones, B.K., Ahmad, C.S., Hung, C.T., Ateshian, G.A., 2015. Wear and damage of articular cartilage with friction against orthopedic implant materials. J. Biomech. 48 (10), 1957–1964.

Pan, Y.-S., Xiong, D.-S., Ma, R.-Y., 2007. A study on the friction properties of poly (vinyl alcohol) hydrogel as articular cartilage against titanium alloy. Wear 262 (7–8), 1021–1025.

Pawaskar, S.S., Fisher, J., Jin, Z., 2010. Robust and general method for determining surface fluid flow boundary conditions in articular cartilage contact mechanics modeling. J. Biomech. Eng. 132 (3), 031001.

Pawaskar, S.S., Ingham, E., Fisher, J., Jin, Z., 2011. Fluid load support and contact mechanics of hemiarthroplasty in the natural hip joint. Med. Eng. Phys. 33 (1), 96–105.

Putignano, C., Burris, D., Moore, A., Dini, D., 2021. Cartilage rehydration: The sliding-induced hydrodynamic triggering mechanism. Acta Biomater. 125, 90–99.

Rajankunte Mahadeshwara, M., Al-Jawad, M., Hall, R.M., Pandit, H., El-Gendy, R., Bryant, M., 2024. How do cartilage lubrication mechanisms fail in osteoarthritis? A comprehensive review. Bioeng. 11 (6), 541.

Rossetti, D., 2022. Early Biological Response of Articular Cartilage to Hemiarthroplasty Wear (Ph.D. thesis). The University of Western Ontario (Canada).

Sadeghi, H., Shepherd, D., Espino, D., 2015. Effect of the variation of loading frequency on surface failure of bovine articular cartilage. Osteoarthr. Cartil. 23 (12), 2252–2258.

Schätti, O.R., Gallo, L.M., Torzilli, P.A., 2016. A model to study articular cartilage mechanical and biological responses to sliding loads. Ann. Biomed. Eng. 44, 2577–2588.

Schmidt, T.A., Gastelum, N.S., Nguyen, Q.T., Schumacher, B.L., Sah, R.L., 2007. Boundary lubrication of articular cartilage: role of synovial fluid constituents. Arthritis Rheum. 56 (3), 882–891.

Schwartz, C.J., Bahadur, S., 2007. Investigation of articular cartilage and counterface compliance in multi-directional sliding as in orthopedic implants. Wear 262 (11–12), 1315–1320.

Shim, J.J., Maas, S.A., Weiss, J.A., Ateshian, G.A., 2021. Finite element implementation of biphasic-fluid structure interactions in FEBio. J. Biomech. Eng. 143 (9), 091005.
Soltz, M.A., Ateshian, G.A., 1998. Experimental verification and theoretical prediction of cartilage interstitial fluid pressurization at an impermeable contact interface in confined compression. J. Biomech. 31 (10), 927–934.
Sophia Fox, A.J., Bedi, A., Rodeo, S.A., 2009. The basic science of articular cartilage: structure, composition, and function. Sport. Heal. 1 (6), 461–468.
Tan, W.S., Moore, A.C., Stevens, M.M., 2023. Minimum design requirements for a poroelastic mimic of articular cartilage. J. Mech. Behav. Biomed. Mater. 137, 105528.
Trevino, R.L., Stoia, J., Laurent, M.P., Pacione, C.A., Chubinskaya, S., Wimmer, M.A., 2017. Establishing a live cartilage-on-cartilage interface for tribological testing. Biotribology 9, 1–11.
Unsworth, A., Dowson, D., Wright, V., 1975a. The frictional behavior of human synovial joints—part I: natural joints.
Unsworth, A., Dowson, D., Wright, V., 1975b. Some new evidence on human joint lubrication. Ann. Rheum. Dis. 34 (4), 277–285.
Van Herck, P., Vanhaecht, K., Deneckere, S., Bellemans, J., Panella, M., Barbieri, A., Sermeus, W., 2010. Key interventions and outcomes in joint arthroplasty clinical pathways: a systematic review. J. Eval. Clin. Pract. 16 (1), 39–49.
Voinier, S., Moore, A., Benson, J.M., Price, C., Burris, D.L., 2022. The modes and competing rates of cartilage fluid loss and recovery. Acta Biomater. 138, 390–397.
Weber, M., Renkawitz, T., Voellner, F., Craiovan, B., Greimel, F., Worlicek, M., Grifka, J., Benditz, A., 2018. Revision surgery in total joint replacement is cost-intensive. BioMed Res. Int. 2018.
Williams, P.T., 2013. Effects of running and walking on osteoarthritis and hip replacement risk. Med. Sci. Sports Exerc. 45 (7), 1292.
Willing, R., Lapner, M., King, G.J., Johnson, J.A., 2014. In vitro assessment of the contact mechanics of reverse-engineered distal humeral hemiarthroplasty prostheses. Clin. Biomech. 29 (9), 990–996.
Wu, Y., Ferguson, S.J., 2017. The influence of cartilage surface topography on fluid flow in the intra-articular gap. Comput. Methods Biomech. Biomed. Eng. 20 (3), 250–259.
Yang, F., Zhao, J., Koshut, W.J., Watt, J., Riboh, J.C., Gall, K., Wiley, B.J., 2020. A synthetic hydrogel composite with the mechanical behavior and durability of cartilage. Adv. Funct. Mater. 30 (36), 2003451.
Zhao, Z., Li, Y., Wang, M., Zhao, S., Zhao, Z., Fang, J., 2020. Mechanotransduction pathways in the regulation of cartilage chondrocyte homoeostasis. J. Cell. Mol. Med. 24 (10), 5408–5419.